ORIGINAL ARTICLE

Characterization of SIEMENS Symbia T SPECT camera in Monte Carlo simulation environment

Xianling Dong[1], Mahmud Iqbal Saripan[2]*, Rozi Mahmud[3], Syamsiah Mashohor[2], Aihui Wang[4]

*Faculty of Engineering, Universiti Putra Malaysia, Serdang, Malaysia.

ABSTRACT

Background: Monte Carlo N-Particle code, version 5 (MCNP5) is a general-purpose Monte Carlo code and it can be used for the design of imaging systems. In this paper, a realistic single photon emission computed tomography (SPECT) model was developed referred to the SIEMENS Symbia T imaging system.

Methods: The most important components of the SPECT camera were modeled, especially a low-energy high-resolution collimator with hexagonal-hole was simulated as closely as possible to its shape and dimensions. The photoelectric effect, Compton and coherent scattering were included in the gamma transport process. In order to validate the SPECT model, specifications in terms of intrinsic spatial resolution, energy resolution, sensitivity, system spatial resolution, and tomography spatial resolution were calculated in comparison with experimental data.

Results: Overall results showed good agreements between the simulations and experimental results provided by SIEMENS. The simulated intrinsic resolution and energy resolution matched well with experimental data. The sensitivity measurements from simulation data yielded higher values. For the system spatial resolution, it differed about 3% compared with the experimental result. The tomographic results showed differences of 5.9%, 5.6%, 0.3%, 10.7%, and 0.2% for the five average resolutions, respectively.

Conclusion: In summary, the results demonstrated the flexibility and accuracy of MCNP5 to simulate the basic features of SIEMENS Symbia T SPECT Camera and exemplified its potential benefits in protocol optimization and in system design.

Keywords: Monte Carlo simulation, MCNP5, SPECT.

INTRODUCTION

The aim of nuclear medicine is to obtain an image of the distribution of the radionuclide administrated into the patient body. This is accomplished by detecting the emissions with external scintillation crystals. Single photon emission computed tomography (SPECT) imaging is one of the established modalities, which are commonly used in modern hospitals. Compared to the structural imaging modalities, such as mammography, ultrasound and magnetic resonance imaging, SPECT provides functional information of the organ, which can show the lesion at an early stage [1,2].

Monte Carlo method is widely applied in statistical process in medical physics because of the stochastic nature of radiation emission, transport, and detection processes. It was first used by H. O. Anger to simulate the physical response of the new scintillation camera and then has been applied in a very wide range of problems which could not be easily handled by experimental or analytical approaches. Many efforts have been done to show the ability of Monte Carlo method in SPECT imaging systems and it is of great use for optimizing the design of SPECT imaging systems and improving the accuracy of reconstructed images [3–6].

Currently, several Monte Carlo codes are available and they can be classified into two main groups. The first group is called generic codes, which are significantly developed to meet the needs for high-energy physics experiments, including electron gamma shower [7], Monte Carlo N-Particle code (MCNP) [8], penetration and energy loss of positrons and electrons [9], and geometry and tracking [10]. The second one is called specific application codes, which are developed for the needs of medical applications, such as simulation of SPECT [11], simulation system for emission tomography [12], GATE [13], and so on. Due to long-term existent and support, the first group codes are widely used in the optimization and system design of SPECT system.

A SPECT model of a dual-headed Philips AXIS camera was simulated by Assié et al. [14]. Saripan et al. [15] simulated the Toshiba GCA-7100A gamma camera by MCNP5. Trionix TRIAD triple-head SPECT camera was simulated based on GATE [16]. SIEMENS E.CAM SPECT camera was simulated based on SIMIND [17] and GATE [13]. Using a point source,

Address for correspondence
Mahmud Iqbal Saripan
*Faculty of Engineering, Universiti Putra Malaysia, Serdang, Malaysia.
Email: iqbal@upm.edu.my

Full list of author information is available at the end of the article.

Received: 12 November 2018
Accepted: 05 December 2018

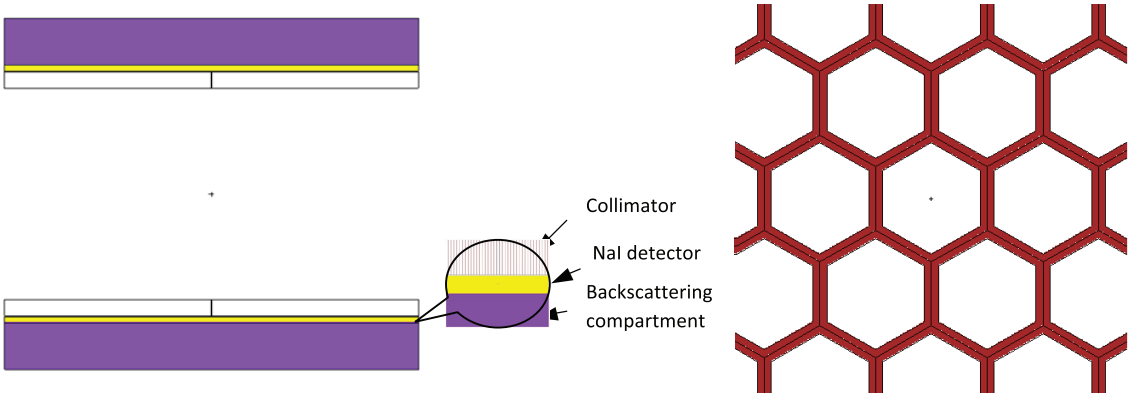

Figure 1. (a) Geometry of dual-head SPECT camera and (b) Geometry of hexagonal-hole collimator, viewed by MCNP Visual Editor (VisEd).

the simulation validity was done by comparison of measured specifications with experimental data in terms of the energy spectrum, energy resolution, spatial resolution, and sensitivity. The basic features of GE Millennium MG SPECT camera were presented by GATE [18]. A point source of 99mTc was used at various positions during static imaging and tomographic acquisitions. Comparisons were made regarding the measurement of sensitivity and spatial resolution both in the planar and tomographic imaging.

MCNP is a general-purpose Monte Carlo code and accounts for all the interaction types: photoelectric absorption, Compton scattering, coherent scattering, and pair production. Furthermore, important features make MCNP very versatile and easy for complicated geometry structures. In this study, we intended to develop a simulated SPECT system model based on MCNP5 and characterized its specifications in terms of intrinsic spatial resolution, energy resolution, sensitivity, system spatial resolution, and tomography spatial resolution.

MATERIALS AND METHOD

Basic characteristics of SIEMENS Symbia T SPECT camera

The SIEMENS Symbia T camera is a dual-head SPECT camera, which consists of a removable low-energy high-resolution (LEHR) collimator, a scintillation crystal, a light guide, and an array of photomultiplier tubes (PMTs) [19]. As shown in Figure 1, the LEHR collimator is a slab filled with lead material, parallel hexagonal holes with cells of 0.111 cm hole diameter, 0.016 cm septal thickness, and 2.405 cm height. The detector is filled with sodium iodide (NaI) and 0.9525 cm in thickness, 53.3 × 38.7 cm^2 in area with density 3.67 g/cm^3. The composition of all materials used in the simulation, shown in Table 1, was assigned according to International Commission on Radiation Units and Measurements report [20].

A light guide made of thick crown glass was positioned behind the detector, followed by PMTs. However, it was not practical to simulate explicitly each of the components behind the scintillation crystal; the combined effect could be approximated by adding a single layer of material called "backscattering compartment," which consists of a Pyrex® slab with density of 1.4718 g/cm^3 and thickness of 6.6 cm [21].

Position determination and blurring strategy

Previous study showed the strategy of position determination and position blurring; particle track output file [named as Particle track (PTRAC)] linked with tally F8 was generated by MCNP to get the location of the photon and energy deposited. An ideal detector produced a delta pulse for each incident photon. However, the real deposited energy was spread due to the statistical variations in the PMTs, which led a Gaussian-like pulse instead of a delta one. Full-wide half-maximum (FWHM) of the response was used to determine the realistic energy blurring function given by Beattie and Byrne [22]:

$$FWHM = k_1 \times E^{1-k_2} \qquad (1)$$

Table 1. Material compositions for each component used in the simulation.

Material	Density (g/cm^3)	Atomic number	Fraction by weight
Lead	11.35	Ld-82	1
Sodium Iodide	3.667	Na-11	0.153373
		I-53	0.846627
Pyrex®	1.4718	B-5	0.040064
		O-8	0.539562
		Na-11	0.028191
		Al-13	0.011644
		Si-14	0.377220
		K-19	0.003321

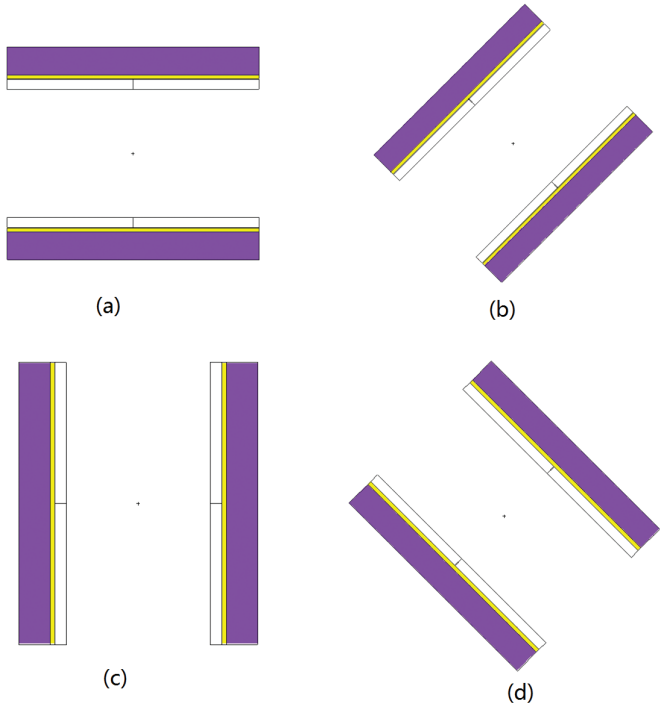

Figure 2. Simulated SPECT scanner rotated clockwise, viewed by VisEd. (a) 0°; (b) 45°; (c) 90°; and (d) 135°.

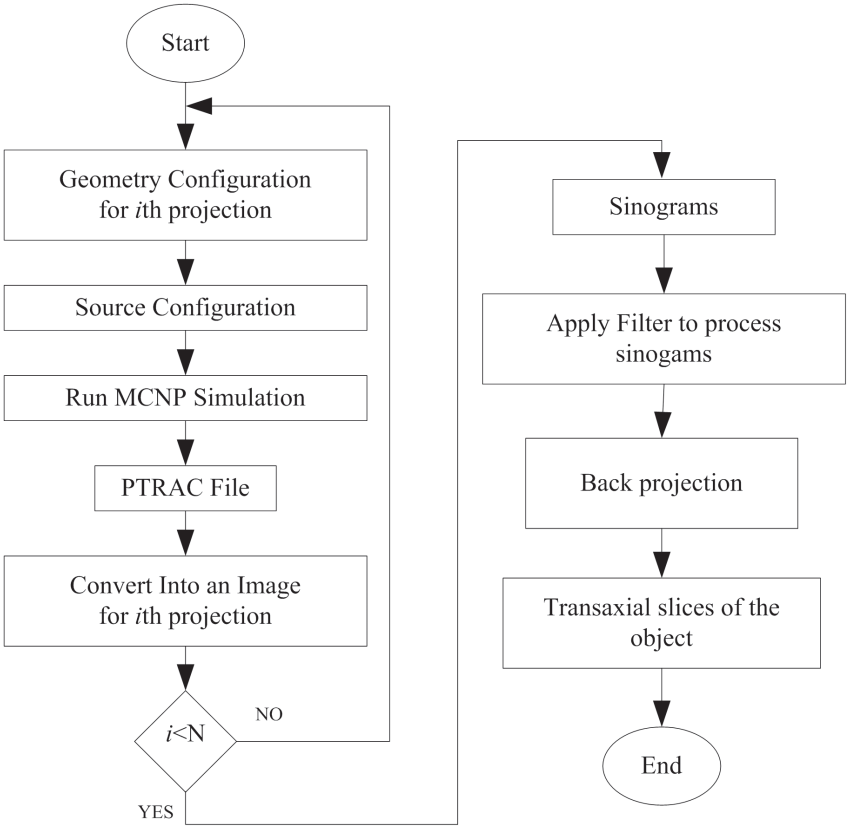

Figure 3. Flowchart for the process of reconstructed slice formation, N is number of projections.

The fitting values k_1 = 0.35 and k_2 = 0.23 were obtained in a preliminary experiment [15] conducted at the Royal Surrey County Hospital and a relationship was derived using experimental values obtained by plotting FWHM of the photopeak for various radioisotopes (201Tl, 57Co, 99mTc, and 51Cr). k_1 and k_2 values were determined in the case where the simulated energy spectra were similar structure to that of experimental ones.

The centroid of the positions for the photon interaction in the scintillation crystal was calculated and the summed energy was considered to be deposited at this site according to Eqs. 2 and 3 [23]:

$$X_i = \frac{\left(\sum_{j=1}^{m_i} x_{ij} \times E_{ij}\right)}{\sum_{j=1}^{m_i} E_{ij}} \quad (2)$$

$$Y_i = \frac{\left(\sum_{j=1}^{m_i} y_{ij} \times E_{ij}\right)}{\sum_{j=1}^{m_i} E_{ij}} \quad (3)$$

where m_i is the total number of event occurred in the detector for the i^{th}photon history. (x_{ij}, y_{ij}) and E_{ij} are the coordinates and deposited energy for the j^{th} event of the i^{th} photon history.

Due to the light sharing in the PMTs, position blurring was applied for a realistic scintillation camera and the photons lied within ±10% energy window were determined and used to form a grayscale image. In this stage, the image obtained was called projection.

The essence of SPECT is to obtain many projections from different angles around the object being imaged. In this study, all the experiments for image reconstruction obtained 120 projections at equally spaced angles between 0° and 360°. It was tough work to construct geometries of SPECT system for every angle, whereas, the features of repeated structure card made it easy to construct this geometry only once but could be rotated at any angle. Figure 2 shows the simulated SPECT scanner in different angles.

Sinograms were obtained from each row of the projection image. Then, filter such as Ramp [24] was used to process the sinograms. Then, the slices of the object were constructed by back

Table 2. Tools used for simulated SPECT camera.

Components	Tool
Detector	MCNP5
Collimator	MCNP5
PMT	MCNP5
Pulse Arithmetic	MCNP5 & Matlab
Pulse height analyzer	MCNP5 & Matlab
Energy blurring	Matlab
Position blurring and determination	Matlab
Image filtering	Matlab
Back projection	Matlab

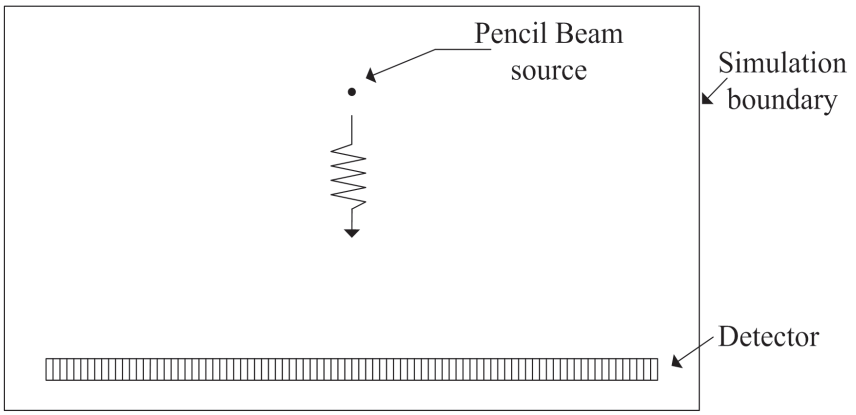

Figure 4. Simulation environment of scintillation camera.

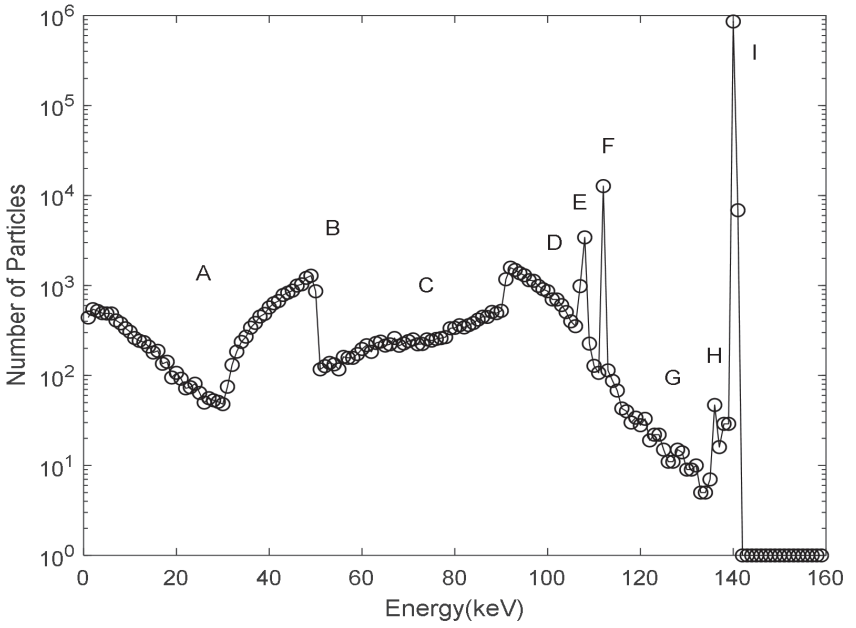

Figure 5. Energy deposited in the NaI detector.

projection with 64 × 64 matrix size. The overall flowchart for the process of reconstructed slice formation was shown in Figure 3. Table 2 shows a summary of the tools used. Energy CUT and Photon CUT values were set to be 1 keV. The most important components of this camera were constructed by MCNP5; pulse arithmetic and pulse height analyzer were calculated by Matlab program using PTRAC file, while the rest algorithms were implemented by Matlab program.

Model validation

Since the experimental results provided by SIEMENS were obtained according to the National Electrical Manufacturers Association (NEMA) protocols, the following properties of this camera were determined according to the same guideline in order to validate the SPECT model: intrinsic spatial resolution, energy resolution, sensitivity, system spatial resolution, and tomography spatial resolution [15,17,18,25]. 99mTc radiation source was mainly used for the measurement of performance characteristic [26]. Point source was defined as monoenergetic gamma emitter of 140 keV, with an isotropic angular distribution emission of gamma photons; 10^7 photons were simulated for point source [3,27]. A pencil beam source was a point source, which only emits only in one direction, and a line source is parallel to the axis of rotation and placed at 10 cm from the face of collimator.

Intrinsic spatial resolution

Intrinsic spatial resolution of the SPECT camera was calculated with a pencil beam source, positioned at the top of detector [23], 10 cm from the crystal surface, shown in Figure 4. In this experiment, no collimator was used in the purpose of examining intrinsic spatial resolution. The simulation boundary was used to specify the limit of the simulated environment.

An image profile across the middle of the generated image was plotted and

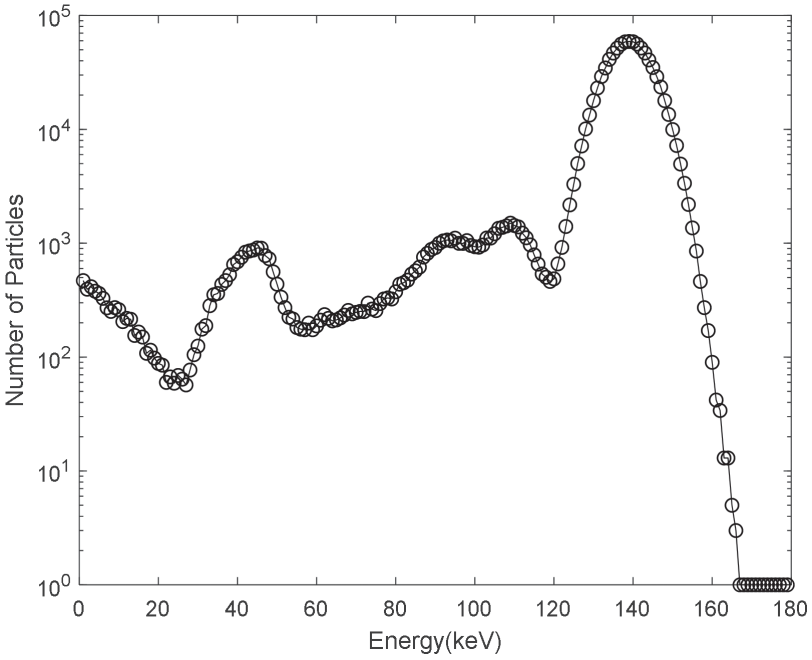

Figure 6. Energy spectrum after blurring.

the resulting distribution was fitted with Gaussian function to measure the FWHM of the point source.

System spatial resolution without scattering

Following the method of NEMA, system spatial resolution without scattering was calculated with line sources. The collected data were summed parallel to the direction of the line source to form line spread functions of width 30 mm or less and calculate the FWHM. Meanwhile, it is also estimated by simulation for the point source placed at different distances (5, 10, 15, 20, 25, and 50 cm) from the surface of the LEHR collimator in ±10% energy window.

Energy resolution

Energy resolution is a term that could characterize the capability of a SPECT camera to distinguish between photons of different energies, especially between primary and scattered radiation [17,18]. It is also commonly quantified as the FWHM of the photopeak, measured in energy units [28]. We used the same method to fit the energy spectrum with Gaussian function to determine the energy resolution $FWHM_E$. Therefore, it shall be expressed as the ratio of the width of photopeak ΔE to the photopeak center energy E_0, stated as a percentage [29]:

$$FWHM_E(\%) = \frac{E}{E_0} \times 100\% \quad (4)$$

Sensitivity

Sensitivity is another important term, which expresses the probability of detecting a photon incident on the detector. It is determined by taking ratio of the detected counts per minute in the selected energy window per unit activity in the source [29]. It is usually estimated by simulating the point source placed at different distances (5, 10, 15, 20, 25, and 50 cm) from the surface of the LEHR collimator in ±10% energy window [18]. The acquisitions at different distances are used to evaluate if the Monte Carlo model could account for sensitivity and spatial resolution resulting from these differences. In this simulation, 10^7 photons were used, which simulated a 99mTc point source with an activity of 1 MBq (27 µCi) with a scan time of 10s. Point source sensitivity was calculated in counts per minutes per µCi (cpm/µCi), by dividing the total number of photon counts per minutes by the activity of the point source.

Tomographic spatial resolution

Tomographic spatial resolution is defined in terms of the FWHM of a point source in the reconstructed slice, which determines the sharpness of the image, as in all types of imaging. It is often affected by position, for example, source distance from the axis of rotation within the slice plane [28]. Therefore, the reconstructed spatial resolution of the system was calculated at three specified points according to protocols of NEMA.

RESULTS AND DISCUSSION

Energy resolution

The energy spectrum was shown in Figure 5. The graph shows various features in the deposited energy, which have been labeled from A to I to make the explanation easier. Section A was from 0 to 50 keV where Compton scattering happened [30]. Peak point B at 50 keV and peak point D at 90 keV showed the effect of the backscattering. Next, section C and G were due to the effect of multiple Compton scattering. Then, peak point E at 107.9 keV and peak point F at 112 keV were attributed to X-rays that escaped the crystal, known as the Iodine escape peaks. Finally, the effect of photoelectric absorption created peak point H at 135 keV and I at 140 keV. Energy spectrum acquired accounted for three interaction types: Compton scattering, coherent scattering, and photoelectric absorption, which showed good agreement with what was described in the literature.

Due to the statistical variations in the PMTs, the real deposited energy was spread, which led to a Gaussian-like pulse instead of a delta one. As shown in Figure 6, the blurred spectrum was similar to the one before blurring; only the delta pulses were transformed into Gaussian-like ones.

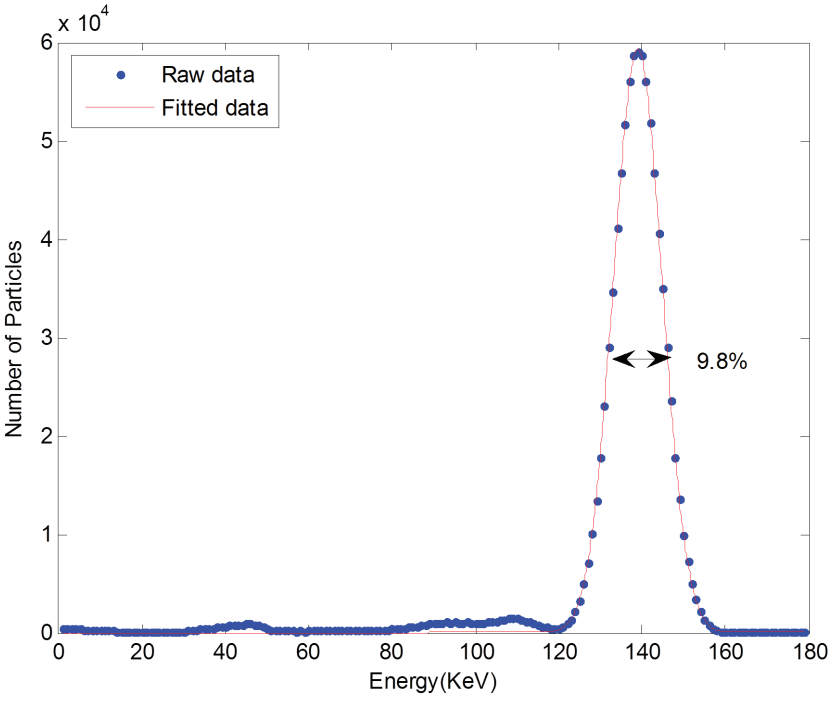

Figure 7. Blurred energy spectrum, fitted by Gaussian function.

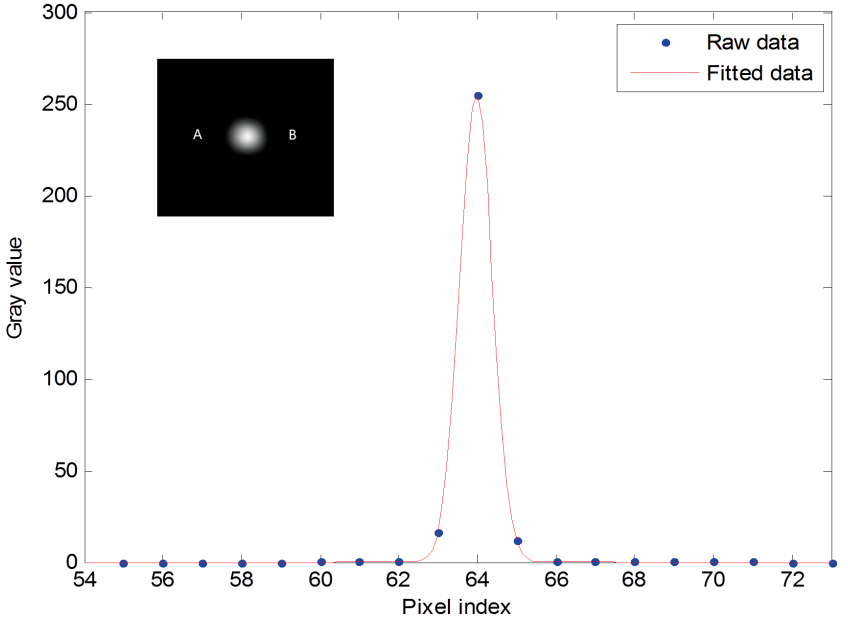

Figure 8. Generated image profile across the middle of the image from point A to point B fitted by Gaussian function. The inset is the simulated image.

The blurred energy spectrum fitted by Gaussian function was shown in Figure 7. The mean and standard error of energy resolution that determined from simulated spectrum were 9.8% and 0.006%, respectively, which matched well with 9.9% claimed by the manufacturer.

Intrinsic spatial resolution

The mean and standard error of intrinsic spatial resolution were 3.7 and 0.002 mm, respectively, which came out with the same value as that of SIEMENS Symbia T SPECT camera when the simulated image profile was fitted into Gaussian function, shown in Figure 8.

System spatial resolution and sensitivity

System spatial resolution and sensitivity were estimated by 99mTc point source at different distances from the surface of collimator; the result was shown in Table 3. System spatial resolution became poor when the source-to-collimator distance increased. On the other hand, sensitivity kept almost the similar value when the number of counts was calculated in the entire detector area.

As the source is moved farther away from the collimator, the efficiency with which radiation was transmitted through any one collimator hole decreased, but the number of holes through which radiation can pass to reach the detector increased. These two effects cancelled each other. Therefore, sensitivity did not change a lot with source-to-collimator distance [29]. However, as the distance reached to 50 cm, sensitivity decreased due to the limit size of detector. As can be seen, sensitivity determined in simulation was 233 cpm/μCi, which was higher than the experimental results 202 cpm/μCi. The discrepancy may be due to the fact that the implemented gamma camera model did not take into account small areas (dead spaces) between PMT, acquisition dead time, and signal overlap in the detector, which was in agreement with the previous study [17,18], where the simulated one yielded higher sensitivity than experimental one. The overall results verified the ability of the simulated camera model that could account for sensitivity and system spatial resolution resulting from different source-to-collimator distance.

Apart from the point source, 99mTc line source was also used to determine system spatial resolution. The experiment was set up according to the method recommend by the NEMA. The collected image shown in Figure 9 was summed parallel to the direction of the slits to form line spread function and the measured FWHM was 7.3 ± 0.08 mm,

Table 3. System spatial resolution and sensitivity at different distance.

Distance(cm)	Spatial resolution (mm)		Sensitivity (cpm/μCi)	
	Mean	SD	Mean	SD
5	5.2	0. 2	238	7
10	7.4	0.3	233	5
15	10.0	0.2	233	9
20	11.2	0.3	231	6
25	13.3	0.2	231	8
50	19.3	0.3	220	6

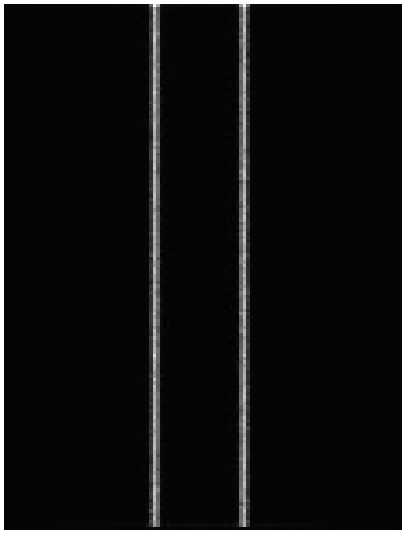

Figure 9. Line source image for system spatial resolution at 10 cm.

which differed about 3% compared with the experimental result.

Tomographic spatial resolution

Three orthogonal slices, each containing an image of the three point sources, were reconstructed from raw projection data using filtered back projection (FBP) with Ramp filter; the result was shown in Figure 10. Slices of these points were reconstructed in transaxial, sagittal, and coronal plane in order to calculate the tomographic spatial resolution.

Table 4 summarizes the comparison of tomographic spatial resolution between the simulated result and experiment ones provided by the manufacturer. The results showed differences of 5.9%, 5.6%, 0.3%, 10.7%, and 0.2% for the five average resolutions, respectively. A possible explanation for these differences may be related to the specific settings and acquisition conditions used by the manufacturer (e.g., the actual size of points source). However, the simulated values met the specifications with the experimental ones. It means the simulated SPECT model could account for the tomographic spatial resolution for different positions within the slice plane.

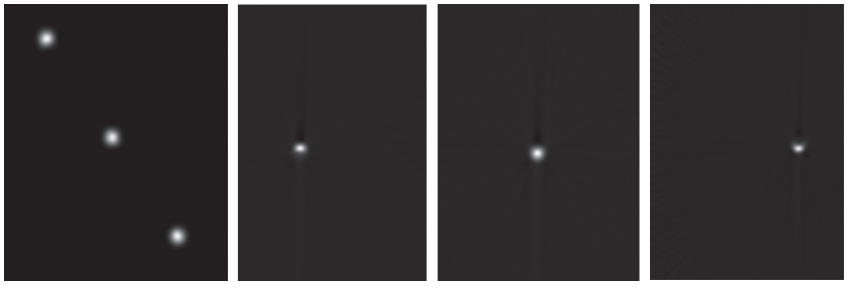

Figure 10. Tomographic results (a) projection of three point sources; (b) reconstructed slice of upper left point in transaxial plane; (c) reconstructed slice of middle point; (d) reconstructed slice of lower right point.

Table 4. Specifications obtained by simulation and experiment provided by the manufacturer.

Specifications	Simulation	Manufacturer
Detector specifications		
Intrinsic spatial resolution	3.7 ± 0.002 mm	≤3.8 mm
Intrinsic energy resolution	9.8% ± 0.006%	≤9.9%
Detector with collimator specifications		
System spatial resolution without scatter at 10 cm	7.3 ± 0.08 mm	≤7.5 mm
System sensitivity (LEHR at 10cm)	233 ± 4.5 cpm/μCi	202 cpm/μCi
Tomography specifications		
Reconstructed spatial resolution without scatter at 15 cm radius (LEHR)	FBP	
Central transaxial	9.6 ± 0.05 mm	≤10.2 mm
Central axial	10.2 ± 0.07 mm	≤10.8 mm
Peripheral radial	9.8 ± 0.03 mm	≤9.8 mm
Peripheral tangential	7.5 ± 0.08 mm	≤8.4 mm
Peripheral axial	9.0 ± 0.02 mm	≤9.0 mm

CONCLUSION

How well simulations can predict the physical response of the camera is often examined by comparing the simulated and empirical values of some parameters that characterize the physical performances of the system; the parameters can be experimentally measured. If it accurately reproduces the response of the experimental system, then it is considered to be validated. The parameters of interest that commonly used are the intrinsic resolutions, spatial resolution, sensitivity, as well as tomographic specifications obtained in specific configurations.

Simulation setup was designed according to NEMA standards, which are commonly recognized by many institutions. Based on the results presented in this study, the simulated SPECT model was well matched with the performance of experimental system, which showed the ability of MCNP to model SPECT imaging systems. However, the model deserves to be improved. PMTs geometry, location, physical properties, and system electronics should be included in the model in order to get effects as acquisition dead space and dead time adequately modeled. Future works focus on the accuracy of the simulated model for the applications of software and hardware optimization as well as quantitative analysis of images.

List of abbreviations

FBP	Filtered back projection
FWHM	Full-wide half-maximum
LEHR	Low-energy high-resolution
NEMA	National Electrical Manufacturers Association
SPECT	Single photon emission computed tomography

Funding

This work was supported by the Educational Commission of Hebei Province of China under Grant No. NQ2018066, High level talent research start-up fund of Chengde Medical University under Grant No. 201802, and the Ministry of Science, Technology and Innovation (UPM) under Science fund Grant number 5450786 (06-01-04-SF2157).

Conflict of interests

The authors declare that there is no conflict of interest regarding the publication of this article.

Consent for Publication

Not applicable.

Ethical Approval

Not applicable.

Author details

Xianling Dong[1], Mahmud Iqbal Saripan[2], Rozi Mahmud[3], Syamsiah Mashohor[2], Aihui Wang[4]

1. Department of Biomedical Engineering, Chengde Medical University, Chengde, China
2. Faculty of Engineering, Universiti Putra Malaysia, Serdang, Malaysia
3. Faculty of Medicine and Sciences, Universiti Putra Malaysia, Serdang, Malaysia
4. Department of Nuclear Medicine, Affiliated Hospital, Chengde Medical University, Chengde, China

REFERENCES

1. Suwijn SR, de Bruin K, de Bie RMA, Booij J. The role of SPECT imaging of the dopaminergic system in translational research on Parkinson's disease. Parkinsonism Relat Disord. 2014;20 Suppl 1:S184–6. https://doi.org/10.1016/S1353-8020(13)70043-9
2. Brandon D, Alazraki A, Halkar RK, Alazraki NP. The role of single-photon emission computed tomography and SPECT/computed tomography in oncologic imaging. Semin Oncol. 2011;38:87–108. https://doi.org/10.1053/j.seminoncol.2010.11.003
3. Saad WHM, Roslan RE, Mahdi MA, Choong WS, Saion E, Saripan MI. Monte Carlo design of optimal wire mesh collimator for breast tumor imaging process. Nucl Instrum Methods Phys Res Sect Accel Spectrometers Detect Assoc Equip. 2011;648:254–60. https://doi.org/10.1016/j.nima.2011.05.064
4. Talat D, Guvenis A. Design and evaluation of a breast-specific collimator using response surface methodology and Monte Carlo simulations. IEEE Trans Nucl Sci. 2016;63:98–107. https://doi.org/10.1109/TNS.2015.2484070
5. Hirano Y, Zeniya T, Iida H. Monte Carlo simulation of scintillation photons for the design of a high-resolution SPECT detector dedicated to human brain. Ann Nucl Med. 2012;26:214–21. https://doi.org/10.1007/s12149-011-0561-4
6. Dong X, Saripan MI, Mahmud R, Mashohor S, Wang A. Determination of the optimum filter for 99m Tc SPECT breast imaging using a wire mesh collimator. Pak J Nucl Med. 2017;7:8–17.
7. Yokoi T, Hashimoto T, Shinohara H. Development of EGS-based 3D brain SPECT simulator. Proc Third Int Workshop EGS, Japan; 2005, p. KEK-PROC--2005-3.
8. Elschot M, Lam MG, van den Bosch MA, Viergever MA, de Jong HW. Quantitative Monte Carlo-based 90Y SPECT reconstruction. J Nucl Med Off Publ. 2013;54:1557–63. https://doi.org/10.2967/jnumed.112.119131
9. Espana S, Herraiz JL, Vicente E, Vaquero JJ, Deseo M, Udias JM. PeneloPET, a Monte Carlo PET simulation toolkit based on PENELOPE: features and validation. IEEE Nucl Sci Symp Conf Rec. 2007;4:2597–601.
10. Lee Y-J, Park S-J, Lee S-W, Kim D-H, Kim Y-S, Jo B-D, et al. A Monte Carlo simulation study of the feasibility of a high resolution parallel-hole collimator with a CdTe pixelated semiconductor SPECT system. J Instrum. 2013;8:T03009. https://doi.org/10.1088/1748-0221/8/03/T03009
11. Yanch JC, Dobrzeniecki AB. Monte Carlo simulation in SPECT: Complete 3D modeling of source, collimator and tomographic data acquisition. IEEE Trans Nucl Sci. 1993;40:198–203. https://doi.org/10.1109/23.212341
12. Lu C-C, Lin H-H, Chuang K-S, Dong S-L, Wu J, Ni Y-C, et al. Development and validation of a fast voxel-based dose evaluation system in nuclear medicine. Radiat Phys Chem. 2014;104:355–9. https://doi.org/10.1016/j.radphyschem.2014.01.002
13. Momennezhad M, Sadeghi R, Nasseri S. Development of GATE Monte Carlo simulation for a dual-head gamma camera. Radiol Phys Technol. 2012;5:222–8. https://doi.org/10.1007/s12194-012-0157-2
14. Assié K, Breton V, Buvat I, Comtat C, Jan S, Krieguer M, et al. Monte Carlo simulation in PET and SPECT instrumentation using GATE. Nucl Instrum Methods Phys Res Sect Accel Spectrometers Detect Assoc Equip. 2004;527:180–9. https://doi.org/10.1016/j.nima.2004.03.117
15. Saripan MI, Hashim S, Mashohor S, Adnan WAW, Marhaban MH, Senin HB, et al. Characteristics of multihole collimator gamma camera simulation modeled using MCNP5. AIP Conf Proc. 2008;1017:205–9. https://doi.org/10.1063/1.2940628
16. Min-Jae P, Kwang-Suk P, Jae-Sung L, Yu-Kyeong K, Dong-Soo L. Validation of a GATE Model for the Simulationof a Trionix TRIAD SPECT Camera. J Korean Phys Soc. 2009;55:681–7. https://doi.org/10.3938/jkps.55.681
17. Bahreyni Toossi MT, Islamian JP, Momennezhad M, Ljungberg M, Naseri SH. SIMIND Monte Carlo simulation of a single photon emission CT. J Med Phys Assoc Med Phys India. 2010;35:42–7. https://doi.org/10.4103/0971-6203.55967
18. Vieira L, Vaz TF, Costa DC, Almeida P. Monte Carlo simulation of the basic features of the GE Millennium MG single photon emission computed tomography gamma camera. Rev Esp Med Nucl E Imagen Mol. 2014;33:6–13. https://doi.org/10.1016/j.remn.2013.03.009
19. SIEMENS. SIEMENS SPECT Symbia T: System specifications 2010.
20. ICRU. Tissue substitutes in radiation dosimetry and measurement (Report 44). 1989.
21. de Vries DJ, Moore SC, Zimmerman RE, Friedland B, Mueller SP, Lanza RC. Development and validation of a Monte Carlo simulation of photon transport in an anger camera. IEEE Trans Med Imaging. 1990;9:430–8. https://doi.org/10.1109/42.61758

22. Beattie RJD, Byrne J. A Monte Carlo program for evaluating the response of a scintillation counter to monoenergetic gamma rays. Nucl Instrum Methods. 1972;104:163–8. https://doi.org/10.1016/0029-554X(72)90312-6
23. Dong X, Saad WH, Adnan WA, Hashim S, Hassan NP, Nordin AJ, et al. Simulation of intrinsic resolution of scintillation camera in Monte Carlo environment. IEEE ICSIPA 2013—IEEE Int Conf Signal Image Process Appl; 2013, pp. 11–4.
24. Lyra M, Ploussi A. Filtering in SPECT image reconstruction. Int J Biomed Imaging. 2011;2011:1–14. https://doi.org/10.1155/2011/693795
25. Lee YJ, Ryu HJ, Cho HM, Lee SW, Choi YN, Kim HJ. Simulation studies of a high resolution SPECT system for a photon counting semiconductor detector. IFMBE Proc. 2013;39:1068–71. https://doi.org/10.1007/978-3-642-29305-4_280
26. NEMA. Performance measurements of gamma cameras. 2007.
27. Saripan MI, Petrou M, Wells K. Design of a wire-mesh collimator for gamma cameras. IEEE Trans Biomed Eng. 2007;54:1598–612. https://doi.org/10.1109/TBME.2007.902584
28. IAEA. Quality assurance for SPECT systems. 2009.
29. Cherry SR, Sorenson JA, Phelps ME. Physics in nuclear medicine. 4th ed. Orlando, FL: Grune & Stratton Press; 2012.
30. Saripan MI. Design of a wire-mesh collimator for gamma cameras. Guildford, UK: University of Surry; 2006.